Kinetic Study of the Reaction of Acetaldehyde with OH†

Jinjin Wang, Hongbing Chen, Graham P. Glass,* and R. F. Curl*

Chemistry Department and Rice Quantum Institute, Rice University, Houston, Texas 77005

Received: July 19, 2003; In Final Form: September 19, 2003

The reaction of OH with acetaldehyde in the gas phase has been studied by tunable infrared laser kinetic spectroscopy. As expected, the main channel is the production of water (∼100%). An upper bound of 5% was placed on the yield of CH_3, and the yield of H is estimated as 5 ± 5%. A rate constant of $1.67(10) \times 10^{-11}$ molecules^{-1} cm^3 s^{-1} is obtained for the title reaction, in good agreement with previous measurements. The major product of the reaction, CH_3CO, reacts with O_3, producing CH_3, CO_2, and O_2 in one channel with a rate constant of $1.4(5) \times 10^{-11}$ molecules^{-1} cm^3 s^{-1} and producing CH_3CO_2 and O_2 in the other channel with a rate constant of $3.3(5) \times 10^{-11}$ molecules^{-1} cm^3 s^{-1}.

Introduction

Acetaldehyde is an air pollutant. In the troposphere it reacts to produce peroxyacetyl nitrate (PAN), which exhibits mutagenic activity and is a strong eye irritant.[1] The formation of PAN is believed to be initiated by the reaction of acetaldehyde with OH.[2] Thus the kinetics and products of the reaction of OH with acetaldehyde are of considerable interest. At room temperature, the bimolecular rate constant for the reaction of acetaldehyde with OH is well established.[3] However, serious uncertainties exist concerning the reaction mechanism. For many years, it was assumed that the reaction occurred by abstraction of the weakly bonded aldehydic hydrogen atom

$$OH + CH_3CHO \rightarrow H_2O + CH_3CO \qquad \Delta H = -139.6 \text{ kJ/mol} \quad (1a)$$

although abstraction of a methyl hydrogen

$$OH + CH_3CHO \rightarrow H_2O + CH_2CHO \qquad \Delta H = -102.6 \text{ kJ/mol} \quad (1b)$$

is not ruled out. However, it is well-known that the reaction exhibits a negative temperature dependence that is similar to that displayed by many addition reactions of OH. For this reason, it has been suggested that it occurs by means of an addition−elimination reaction

$$OH + CH_3CHO \rightarrow [CH_3C(OH)HO]^* \rightarrow \text{elimination products} \quad (1c\text{-}d)$$

Energetically allowed channels in addition to (1a) and (1b) include

$$OH + CH_3CHO \rightarrow CH_3 + HCOOH \qquad \Delta H = -106.2 \text{ kJ/mol} \quad (1c)$$

$$\rightarrow H + CH_3COOH \qquad \Delta H = -87.4 \text{ kJ/mol} \quad (1d)$$

where the heats of formation are based upon a recent compilation.[3]

A particularly thorough discussion of the mechanism of the $OH + CH_3CHO$ reaction has been presented by Michael et al.[4] These authors tended to favor an abstraction mechanism. The most compelling argument cited in support of this mechanism was that the addition of O_2 to the reaction system significantly decreased the rate at which OH was consumed. They interpreted this observation as indicating that OH is re-formed in a reaction between CH_3CO and O_2. However, because they were unable to propose a precise mechanism for such a reaction, they concluded by asserting that acetyl radicals are only the most *probable* products of the reaction.

An addition−elimination mechanism for the reaction was postulated by Taylor et al.[5] in 1996. They measured absolute rate coefficients for the reactions of OH with CH_3CHO, CH_3CDO, and CD_3CDO over the temperature range 295−900 K and performed quantum RRK calculations on ab initio potential energy surfaces for both abstraction and addition channels. At low temperatures, they proposed that the dominant mechanism involved addition of OH to form a bound intermediate, which then dissociated by CH_3 elimination.

$$OH + CH_3CHO \rightarrow CH_3 + HCOOH \quad (1c)$$

Their calculations indicated that, at 295 K, H-atom abstraction was only a minor channel, accounting for approximately 10% of the total rate. They indicated that the kinetic isotope measurements supported their proposed mechanism.

In 2000, a very different conclusion was reached by Alvarez-Idaboy et al.[6] on the basis of their ab initio calculations. The results of these authors clearly showed that the reaction occurred by hydrogen abstraction. They further suggested that the reaction occurs via the formation of a prereactive complex in which the hydrogen atom of OH is loosely bonded to the oxygen atom of acetaldehyde. A very recent experimental paper[7] using FTIR analysis of final products also supports the conclusion that abstraction dominates. However, no work has found the nascent reaction products. This is the aim of the present work.

In the present investigation, the reaction of OH/acetaldehyde was studied by using infrared kinetic spectroscopy to measure the relative importance of the channels producing H_2O (abstraction), CH_3 (addition), and H (addition). In addition, strong evidence for reaction between CH_3CO and O_3 was found.

† Part of the special issue "Charles S. Parmenter Festschrift".

10.1021/jp036114p CCC: $25.00
Published on Web 11/05/2003

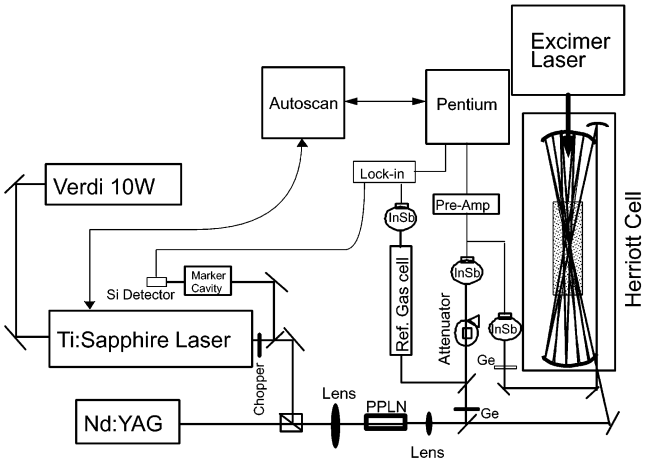

Figure 1. Optical arrangement of the apparatus employed.

In these experiments, OH was produced by the reaction of $O(^1D)$ with a large excess of H_2O using the reaction,

$$O(^1D) + H_2O \rightarrow 2OH \qquad (2)$$

This led naturally into a parallel investigation of the kinetics and products of the reaction between $O(^1D)$ and acetaldehyde, which will be reported in the future.

Experimental Section

The technique of infrared kinetic spectroscopy was employed for this work. These experiments were all carried out in a large excess of helium, which served as a buffer gas, at a total pressure of 10−20 Torr. To investigate the reaction between acetaldehyde and OH, $O(^1D)$ was generated by flash photolysis of a suitable precursor (N_2O, NO_2, or O_3) and then converted to 2OH radicals through its reaction with water in large excess. Because most of the products expected for the reaction of acetaldehyde with OH overlap with possible products of the reaction between $O(^1D)$ and acetaldehyde, the assumption of complete flooding by water had to be checked. An additional concern was the possibility that acetaldehyde might be photolyzed at 193 or 248 nm, the two wavelengths used for $O(^1D)$ production. Fortunately, the absorption cross-sections of acetaldehyde at these wavelengths are very low. Also as is always the case in this kind of experiment, care had to be taken to avoid contaminating the chemistry through product buildup or reagent depletion by keeping the flash repetition rate low and the total gas flow rate high. Apart from these concerns, the essential experimental concerns for these experiments are the measurement of infrared absorption and the measurement of reagent concentrations. These are described below.

Infrared Kinetic Spectroscopy Apparatus and Intensity Measurements. Figure 1 depicts the laser instrumentation. This apparatus is very similar to that used previously[8] for the investigation of the reaction between NH_2 and NO_2 except the 1 m White cell used in those experiments has been replaced by a 2 m (1.83 m actual) Herriott cell based upon the modification of the standard design described by Pilgrim, Jennings, and Taatjes.[9] The Herriott cell was operated at 31 passes. The laser probe only overlaps the photolyzed region in the central portion of the cell giving a total usable path length of ∼20 m (∼0.64 × 31). All infrared frequencies employed were generated by difference frequency mixing of a Coherent AutoscanTi:Sapphire laser with a single frequency Nd:YAG in periodically poled $LiNbO_3$ (PPLN). The line width (about 1 MHz) of the resulting infrared probe was much narrower than the line widths (typically 200 MHz) of individual rovibrational transitions monitored.

To carry out quantitative measurement of the infrared absorbances, the probe IR frequency was scanned over the line in typically 20 MHz steps. At each frequency step, the excimer photolysis laser was fired about 10 times and the entire time profile relevant to the experiment was acquired with a transient digitizer. Time-correlated noise was then removed from the data thus acquired by subtracting the time channel immediately before the excimer firing from the rest of the channels. This substantially denoised data were then analyzed by fitting a Gaussian line shape to the data at each time. Four parameters were fitted: peak height, line width, center frequency, and baseline. For OH, the resulting line widths were in good agreement with the expected Doppler profile, but for CH_3 the line widths were significantly larger than the expected Doppler profile. However, the line shapes observed for CH_3 were still rather satisfactorily Gaussian. We believe the additional broadening over Doppler observed for CH_3 arises from unresolved but still substantially split hyperfine structure. In some situations the line width parameter was known and could be fixed by reducing the fit to three parameters; in some cases the central frequency was also known to reduce the fit to two parameters.

This method for acquiring and treating data has the advantage that if pressure broadening ever becomes significant, the data can be fitted with a Voigt profile and integrated intensities calculated. In carrying out the fitting, the quality of the fit at any time point can be examined. Typically, a number of time points shortly after the flash when the signal is largest are examined. On the basis of these examinations the center frequency and line width can be fixed and the two-parameter fitting is then allowed to proceed automatically into the longer time region where the data are often much noisier. These multiple least-squares fittings also provide the estimated standard deviations of the parameters at each time allowing the peak heights to be plotted with error bars at any or all times.

Reagents and Concentration Measurements. The reaction studied here is relatively fast ($k = 1.67 \times 10^{-11}$ cm^3 s^{-1}), and the preceding $O(^1D)$ reactions are even faster ($k > 10^{-10}$ cm^3 s^{-1}). This means that there is little concern that a minor impurity will consume a significant portion of the radical pool. As radical products also will tend to react rapidly, secondary reactions can be, and on some occasions are, important, but again minor impurities have little impact. Because the helium buffer gas is present at a much higher concentration than any other reagent, an impurity in the helium conceivably might be a problem. However, the helium used was of very high purity (99.999%). Thus standard commercial chemicals were used in this work with no special effort made to purify them. It is well-known that acetaldehyde can polymerize. The polymer product produced at room temperature is the trimer paraldehyde. This (and all other acetaldehyde polymer products) are all much less volatile than monomeric acetaldehyde (bp acetaldehyde 20.8 °C; bp paraldehyde 128 °C). Thus as long as acetaldehyde polymerization is small, there is no reason to be concerned about our observations on acetaldehyde being affected by reactions of paraldehyde (or other polymers).

The partial pressure of water was measured directly by measuring the absorbance of weak water lines. For this purpose, the absorbances of a line of HDO in natural abundance at 3528.808 cm^{-1} and a line of H_2O at 3528.730 cm^{-1} were used. The typical partial pressure of water was approximately 1.1 Torr. The other reagent concentrations were calculated by measuring the flow rates of the reagents and of the helium buffer gas. The

H_2O flow rate could be calculated from the other flow rates, its partial pressure, and the total pressure. The partial pressure of each of the other reagents could then be calculated by dividing its flow rate by the total of all flow rates and multiplying by the total pressure. Flow rates were measured by two different methods. For simple gaseous reagents (He, CH_4, N_2O) flow controllers were used to set the flow. For acetaldehyde and NO_2, the pressure drop in a known volume in known time taking into account the equilibrium $2NO_2 \rightleftarrows N_2O_4$ was used to calculate the flow rate. For ozone, the flow rate was measured by a more complex procedure described below.

In this study, three different sources of $O(^1D)$ were used, the 193 nm photolysis of N_2O, the 248 nm photolysis of O_3 and the 193 nm photolysis of NO_2.

$$N_2O + h\nu\ (193\ \text{nm}) \rightarrow O(^1D)(100\%) + N_2 \qquad (3)$$

$$NO_2 + h\nu\ (193\ \text{nm}) \rightarrow O(^1D)(55\%) + NO \qquad (4)$$

$$O_3 + h\nu\ (248\ \text{nm}) \rightarrow O(^1D)(>90\%) + O_2(^1\Delta_g) \qquad (5)$$

N_2O has an absorption cross section of 9×10^{-20} cm^2 at 193 nm,[10] and a quantum yield for $O(^1D)$ of 1.[11] The absorption cross-section of NO_2 at 193 nm is approximately 3×10^{-19} cm^2,[12] and the quantum yield of $O(^1D)$ is 0.55.[12] The absorption cross section of O_3 at 248 nm is 1.1×10^{-17} cm^2. At 248 nm the yield of $O(^1D)$ from O_3 photolysis is greater than 0.9.[13] In contrast, the absorption cross-section of CH_3CHO is 10^{-20} cm^2 at 248 nm[14] and probably less than 10^{-21} cm^2 at 193 nm (the table referred to above stops at 202 nm where the cross-section is 5.6×10^{-22} cm^2). The typical concentrations of O_3 are usually about a factor of 3 smaller than the CH_3CHO concentrations, implying that the photolysis products of CH_3CHO should be 300 times lower in concentration than $O(^1D)$. At 193 nm N_2O is typically about 5 times larger than the concentration of CH_3CHO; the photolysis products of CH_3CHO should be about 400 times lower in concentration than $O(^1D)$ when N_2O is photolyzed.

N_2O is relatively inert, which reduces secondary chemistry, and its concentration can be easily and reliably measured and does not change during the experiment; furthermore the reaction of $O(^1D)$ with N_2O produces only a small amount of $O(^3P)$, producing instead 2NO or $N_2 + O_2$. Unfortunately, the partial pressure of N_2O in the system had to be kept large (about 250 mTorr) because of its small cross-section. Because N_2O removes $O(^1D)$ rapidly from the system by the reaction,

$$O(^1D) + N_2O \rightarrow 2NO \qquad (6a)$$

$$\rightarrow N_2 + O_2 \qquad (6b)$$

with a total rate constant[15] $k_6 = 1.2 \times 10^{-10}$ cm^3 s^{-1}, large quantities of water were required to compete effectively with N_2O for $O(^1D)$. N_2O was used as the $O(^1D)$ source in the measurement of the CH_3 yield, because of its stable easily calibrated concentration and because CH_3 exhibits no secondary chemistry in the N_2O system.

NO_2 was used for the purpose of searching for H atom products by converting H to OH through the reaction,

$$H + NO_2 \rightarrow OH + NO \qquad (7)$$

but the OH thus produced could not be observed directly by its infrared absorption, because OH reacts rapidly with acetaldehyde. However, as will be described in detail below, once we had determined that H_2O was by far the dominant product of the reaction 1, the OH produced by (7) could be measured as water by a scheme using deuterium labeling. This scheme is complicated by the presence of several other possible sources of D atoms. Fortunately, the total D_2O yield from all sources was small, making the uncertainties in modeling this system less relevant. These issues are discussed in detail below.

Ozone has a large cross-section so that only about 5 mTorr partial pressure of O_3 was required for good signals, but its actual concentration in the cell proved difficult to measure accurately, even making use of its UV absorption as described below. Furthermore, the reaction of $O(^1D)$ with O_3 produces about one $O(^3P)$ atom per reaction through the 50% channel $O(^1D) + O_3 \rightarrow O_2 + O + O$.[15] These O atoms then have the potential of reacting with radical products of reaction 2. Ozone was used extensively in the early stages of this investigation, but most of the results reported here were obtained using N_2O. As will be described below, ozone was found to react with some product of the $OH + CH_3CHO$ reaction probably CH_3CO to produce CH_3 and CO_2.

In summary, reagent concentrations were as follows: The partial pressure of water was about 1 Torr and the acetaldehyde concentration was 10−80 mTorr. O_3 (∼10 mTorr) was used to produce $O(^1D)$ in the measurement of rate constants, and N_2O (∼250 mTorr) was used to produce $O(^1D)$ in the measurement of the CH_3 yield. The He partial pressure was again about 12 Torr. NO_2 partial pressures were typically 10−70 mTorr when it was used in searches for H atom products. When ozone was used, its partial pressure was 3−10 mTorr. All experiments were performed at room temperature (296 K).

In these experiments, hydroxyl radicals were generated by reaction 2. As was stated earlier, reaction 2 is known to be extremely fast ($k_2 = 2.4 \times 10^{-10}$ cm^3 s^{-1}) and produces at least 1.9 molecules of OH for every molecule of $O(^1D)$ consumed. The reaction of $O(^1D)$ with acetaldehyde

$$O(^1D) + CH_3CHO \rightarrow \text{products} \qquad (8)$$

is also extremely fast ($k_8 \sim 3 \times 10^{-10}$ cm^3 s^{-1}), and this reaction produces CH_3 in about 50% yield and H atoms in significant yield. The addition products CH_3 and H of OH with acetaldehyde both have small yields. It was therefore necessary to keep the acetaldehyde concentration much smaller than the H_2O concentration to avoid significant contribution to the CH_3 and H yields through interception of $O(^1D)$ by acetaldehyde. This interception would also reduce the H_2O yield for the reaction. Fortunately, the rate constants of all reactions are well enough known to permit calculation of the effects of interception of $O(^1D)$ by acetaldehyde. This was done through measuring the concentration of reagents and modeling. In addition, it was observed that signals were only affected slightly by large relative changes in the acetaldehyde concentration.

Because the initial concentration of OH was extremely low ($(2-5) \times 10^{13}$ molecule cm^{-3}), the primary products of its reaction with CH_3CHO could in all cases be distinguished from secondary products from their time profiles. Secondary products formed by reactions of primary products with molecules created by photolysis would be expected to grow extremely slowly with half-lives greater than 130 μs, even if they were produced on every gas-kinetic collision. Vibrational relaxation of the reaction products was rapid because OH and CO_2 are efficiently relaxed by water,[16,17] and CH_3 is effectively relaxed by He.[18] As a result, relaxation times for OH, CO_2 and CH_3 were less than 5, 62, and 10 μs, respectively.

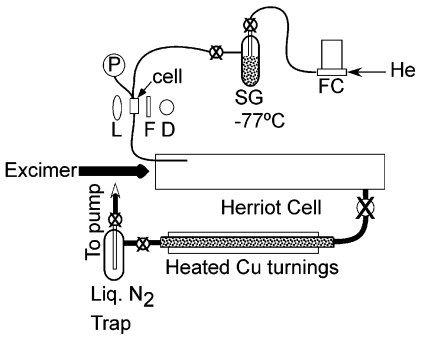

Figure 2. Ozone handling scheme. The ozone is swept from the dry ice cooled silca gel trap containing adsorbed ozone by a controlled He flow. The concentration of the ozone is calculated through measurement at the cell of its absorption of the 254 nm line of Hg using the He flow rate and the pressure at the Hg line monitoring cell. Labels: FC = flow controller, SG = silca gel trap, P = pressure gauge, L = Hg lamp, F = filter passing 254 nm Hg line, D = UV detector. Note the O_3 flow is introduced into the Herriott cell near the point where the excimer and infrared probe beams begin to overlap.

Preparation, Safe Handling, and Measurement of Ozone. Ozone is a dangerous chemical; it is known to have caused serious laboratory accidents. Fortunately, it can be safely stored on silica gel at dry ice temperature. Thus safely obtaining the quantities of ozone desired for this work was as simple as partially filling a trap with silica gel and then flowing the output of an ozonizer through the dry ice cooled trap. A deep blue color indicates the presence of ozone in the trap, and a very crude estimate of the amount trapped can be made from the intensity of the color. Depending upon the loading of the trap, the partial pressure of ozone over the silica gel can range up to perhaps 10 Torr, and it can then be swept into the cell by passing a small flow of He through the trap. Once the ozone has been flowed through the cell, it must be destroyed. A simple, but highly effective method for destroying ozone is to put a brass tube of about a meter length and 1 in. diameter filled with copper turnings and heated to about 140 °C upstream of the liquid nitrogen cooled cold trap. No trace of blue was ever detected in the cold trap. In the initial stages, when we were concerned about how effective the ozone destructor tube might be, we omitted cooling the trap (solid ozone is allegedly very dangerous) and instead put a small piece of latex between the destructor and the trap. Ozone is known to cause rapid disintegration of natural rubber. After running for some time without any change in the latex, we concluded that the ozone destructor was effective and resumed liquid nitrogen trapping.

Because the partial pressure of ozone over the silica gel depends on the ozone loading, some means for measuring the ozone concentration was desirable. In principle, the ozone concentration could be calculated from measurements of the attenuation of the KrF excimer beam as it passes through the cell. However, we thought it more desirable to put a small 1.34 cm long optical cell in the line carrying the helium/ozone mixture and measure the attenuation of the 254 nm line of Hg. Figure 2 shows the ozone handling system. From the total pressure at the optical cell, the flow rate of helium, the 253.7 absorption cross-section of the ozone molecule (1.143×10^{-17} cm^2)[19] and the 254 nm attenuation by ozone, we can calculate the actual flow rate of ozone.

Observations and Results. *(a) Products.* The only primary product of reaction 1 observed with certainty in these experiments was H_2O (in the form of HDO for reasons that will be explained). H atoms were observed indirectly through reaction 7 when NO_2 was the precursor. Additional CH_3 was observed as a secondary product when ozone was used as the source of $O(^1D)$. CO_2 was observed when ozone was used as the source of $O(^1D)$ but is believed to be a secondary product formed by the reaction of CH_3CO with O_3.

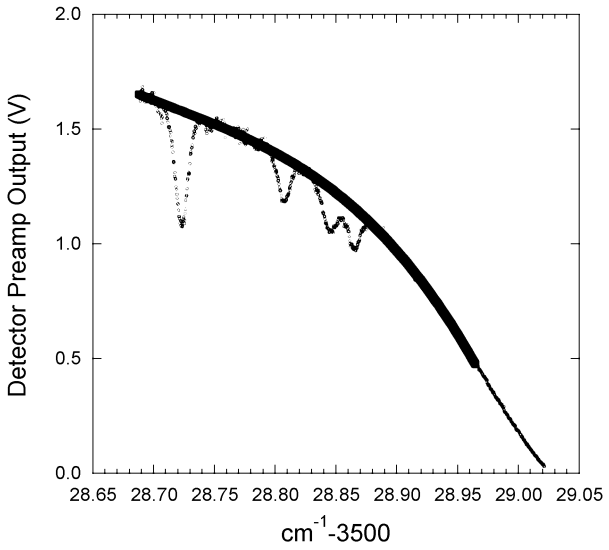

Figure 3. Raw data pure water spectrum in the region of the HDO line used for comparison. The heavy line is the sixth-order polynomial fit of the background. The path length was 58.6 m, and the water vapor pressure was 3.24 Torr. The big dropoff in transmitted laser power toward high frequency is caused primarily by absorption outside the cell from the strong pressure broadened H_2O line at 3529.0559 cm^{-1}, but the contribution of absorption by this line inside the cell is not negligible, as can be seen in Figure 4.

(1) HDO. Because we are using the reaction of $O(^1D)$ with H_2O as our source of OH, observation of H_2O lines would require the use of another OH source, and from previous experience we would expect strong H_2O absorptions in almost any system. Furthermore, the IR beam passes through perhaps 1 m of air and would be greatly attenuated by atmospheric water absorptions. To avoid potentially false conclusions caused by variations in the intensity of an H_2O line as a result of heating by the flash and to avoid the reduction in probe laser intensity caused by atmospheric H_2O absorption, we chose to create OH in the presence of CD_3CDO and observe the HDO line at 3528.808 cm^{-1} created by the following reaction.

$$OH + CD_3CDO \rightarrow HDO + CD_3CO \qquad (1a')$$

The infrared absorbance of the HDO thus produced was compared with the OH signal at 3407.989 cm^{-1} produced with the CD_3CDO flow shut off.

To convert these absorbances into concentrations, the absorption cross-sections of the OH and HDO lines monitored are required. The HDO integrated cross-section can be calculated as 7.24×10^{-21} cm $molecule^{-1}$ from the HITRAN 2000[20] value of 2.25×10^{-24} cm $molecule^{-1}$ using the HITRAN natural abundance (0.00031069) and the integrated OH cross-section of 4.72×10^{-20} cm $molecule^{-1}$ obtained from the same source.[20] As the HDO line chosen for observation is sufficiently intense that HDO in natural abundance is easily detected, we chose to measure the cross-section directly. Figure 3 shows the raw data obtained in scanning over the region of the HDO line. By fitting the baseline in regions where there is no water absorption with a sixth-order polynomial, the 100% transmission line can be determined and A_e, the base e absorbance, calculated. This experimental spectrum is compared in Figure 4 with that predicted from HITRAN for the same pressure and path length.

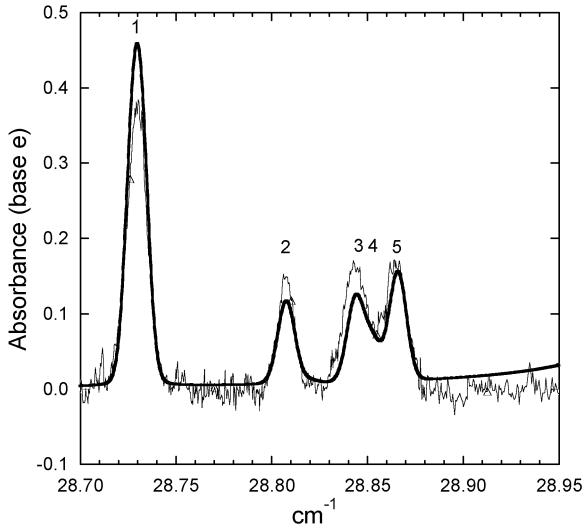

Figure 4. Comparison of the absorbance (base e) observed (noisy) and that predicted by HITRAN (noiseless) for the data of Figure 3. Lines 1, 4, and 5 are H_2O lines and lines 2 and 3 are HDO lines. Line 2 was used in determining the H_2O yield. The contribution of the tail of the strong line at 3529.0559 cm^{-1} has been suppressed for the experimental spectrum by the baseline fitting, but not in the HITRAN spectrum. The experimental frequency scale was adjusted to match HITRAN at the 3528.808 cm^{-1} line. Our data suggest that the very weak line 4 is very nearly superimposed with line 3 instead of being 0.009 cm^{-1} higher in frequency.

The self-broadening coefficients are unknown for these lines, but at the pressure of measurement, 3.84 Torr, pressure broadening should be negligible compared with Doppler broadening. There are clearly differences in intensity between our experimental spectrum and the HITRAN intensities. Though the differences appear small, the line of interest is about 20% stronger than the value from HITRAN. A matter of concern to us was that the acetaldehyde sample becomes contaminated with D_2O through slow exchange of D from CD_3CDO with trace amounts of H_2O. Because our cell had seen D enriched material in the past, we might be tempted to attribute this stronger signal to contamination although normal water had been flowing through cell and had done so for some hours, except that there is also a clear discrepancy in the intensity of the normal line 1, which moreover is not reflected in the intensity of the normal line 5. We estimate that the reproducibility of the HDO cross-section is perhaps ±15%.

There is always an HDO signal present before the flash. Figure 5 compares the pretrigger HDO signal with the post-trigger signal. The difference between the two traces is transient absorption signal. Because the background absorption can be changed by heating the gas as a result of the energy deposited by the flash and the energy released by chemical reaction affecting the transient absorption, an analysis of the effect of pulse heating was carried out and is described in the Appendix. Figure 6 shows the results of this analysis. It is demonstrated in the Appendix that for this line, heating of the gas by 1 K would change the $\log_e$ of the integrated absorbance of the HDO 3528.808 cm^{-1} line by −0.0018. Calculations of the energy deposited by the flash and subsequent reactions indicate a heating of the photolyzed region by about 1 K. This change is imperceptible with our signal-to-noise.

With CD_3CDO present, the extrapolation of the OH signal to the flash point to determine the initial OH concentration is somewhat problematic. Instead, the OH signal in the absence of acetaldehyde, which decays only very slowly (Figure 7), was used. Figure 7 shows OH signal as a function of time in the

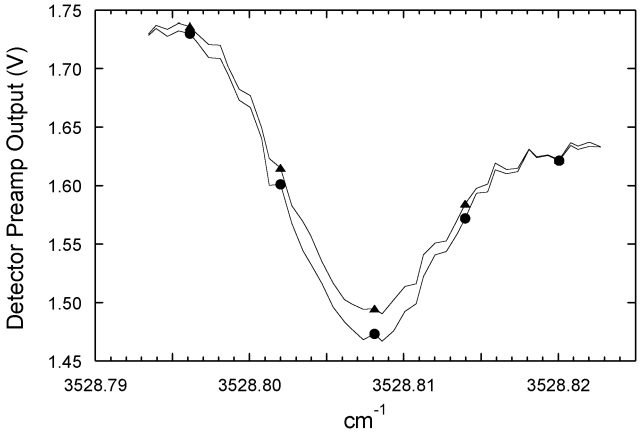

Figure 5. Comparison of the pretrigger (−200 μs to flash average) HDO infrared absorption (▲) with the post-trigger absorption (●) (400−800 μs average). Conditions: He flow 1000 sccm; $P(N_2O) \sim 500$ mTorr, $P(H_2O) \sim 1.1$ Torr, $P(\text{tot}) = 13.5$ Torr; excimer ~ 134 mJ.

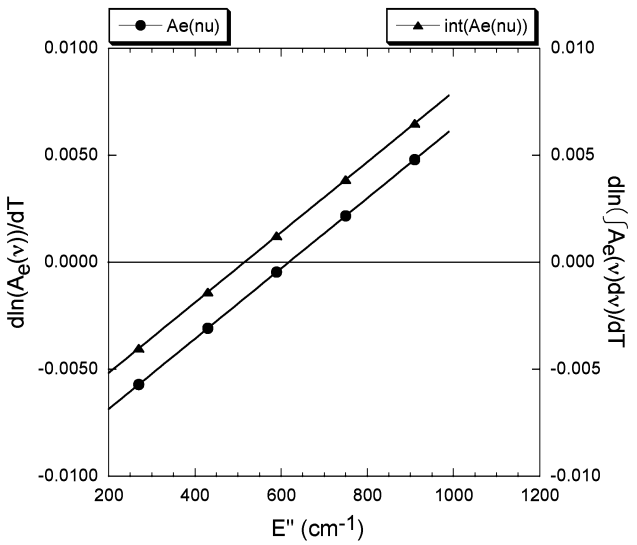

Figure 6. Dependence of temperature derivative of integrated and peak absorption upon E'' at 296 K assuming constant pressure.

absence of CD_3CDO and Figure 8 the HDO signal in its presence at several CD_3CDO concentrations but otherwise identical conditions as a function of time. It is clear from Figure 8 that the HDO yield is approximately 100%. If the HITRAN absorption cross-section for HDO is used, the apparent HDO yield increases to approximately 120%.

Taking into account the uncertainty in the HDO absorption cross-section and the obvious drifts in the data, we estimate the sum of the yields for channel 1a and 1b could be as low as 80%. This would provide as much as 20% of the reaction channels available for the sum of channel 1c, which produces CH_3, and channel 1d, which produces H.

(2) CH_3. The method used to determine the CH_3 yield was to compare the signal magnitude of a CH_3 line with a large excess of water and relatively small amount of acetaldehyde present to the CH_3 signal magnitude with a large excess of CH_4 present and no acetaldehyde. In the first case, $O(^1D)$ is converted almost quantitatively to OH, which then reacts with acetaldehyde to produce CH_3. The partial pressures of H_2O, CH_3CHO, and N_2O are known, as are the rate constants for the reaction of $O(^1D)$ with all these species so that a correction for the incomplete conversion of $O(^1D)$ into OH can be made. The reaction of $O(^1D)$ with acetaldehyde produces CH_3 in large yield,

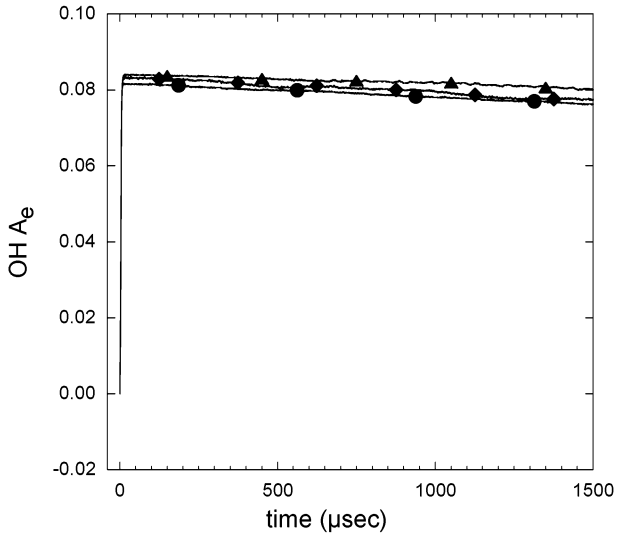

Figure 7. OH absorbance as a function of time in the absence of CD_3CDO for three runs before (●) and after (▲, ◆) HDO measurement. Conditions: He flow 1000 sccm; $P(N_2O) \sim 500$ mTorr, $P(H_2O) \sim 1.1$ Torr, $P(\text{tot}) = 13.7$ Torr; excimer ~ 134 mJ.

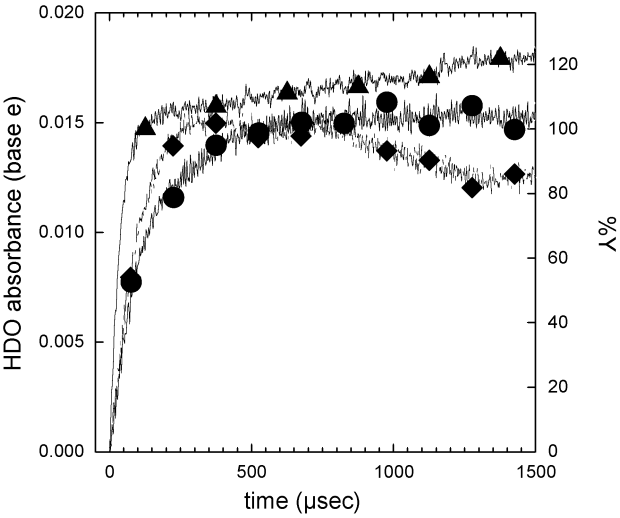

Figure 8. HDO absorbance as a function of time. Conditions: He flow 1000 sccm; $P(N_2O) \sim 500$ mTorr, $P(H_2O) \sim 1.1$ Torr, $P(\text{tot}) = 13.5$ Torr; excimer ~ 134 mJ. Partial pressure of CD_3CDO: (●) 34 mTorr; (▲) 89 mTorr; (◆) 21 mTorr.

but this contribution to the CH_3 signal appears very rapidly and can be distinguished from the slower rise of the CH_3 signal from the reaction of OH with acetaldehyde. The concentration of OH at 2 μs after the flash, a time when essentially all $O(^1D)$ has disappeared, is determined by the competition among acetaldehyde, water, and nitrous oxide for $O(^1D)$

$$[OH]_0 = \frac{2k_2[H_2O]}{k_8[CH_3CHO] + k_2[H_2O] + k_6[N_2O]}[O(^1D)]_0 \quad (9)$$

and the final concentration of CH_3 from channel (1c) is given by

$$[CH_3]_{1c} = (k_{1c}/k_1)[OH]_0 \quad (10)$$

To calibrate the CH_3 signal by finding the CH_3 equivalent of $[O(^1D)]_0$, water and acetaldehyde were replaced by CH_4. The same information is known about the CH_4 and N_2O partial pressures and rates so that similar corrections can be made. The

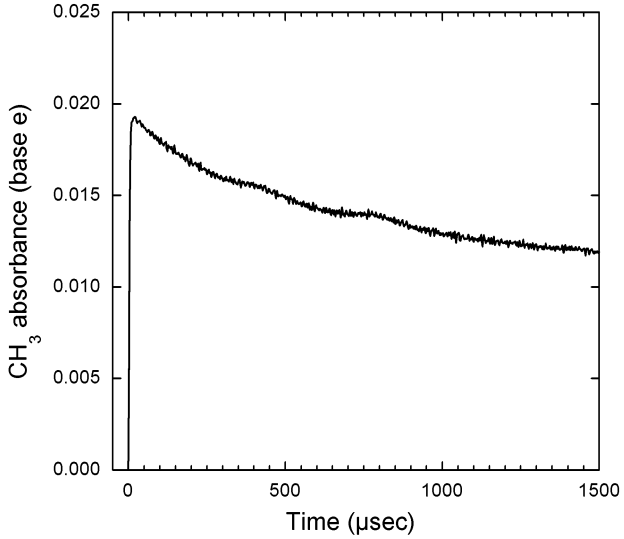

Figure 9. CH_3 signal at 3154.747 cm^{-1} produced by the reaction of $O(^1D)$ with CH_4. Conditions: He flow 1000 sccm; $P(N_2O) \sim 374$ mTorr; $P(CH_4) \sim 1.68$ Torr; $P(\text{total}) \sim 13.6$ Torr; excimer ~ 135 mJ.

reaction between CH_4 and $O(^1D)$ has other channels in addition to

$$CH_4 + O(^1D) \rightarrow CH_3 + OH \quad (11a)$$

The yield of channel 11a is 75%.[15] The $[CH_3]$ expected from (11a) is given by

$$[CH_3]_{11a} = \frac{0.75k_{11}[CH_4][O(^1D)]_0}{k_{11}[CH_4] + k_6[N_2O]} \quad (12)$$

The value of $[O(^1D)]_0$ in (9) and (12) is the same at the same $[N_2O]$ and excimer power so that (9), (10), and (12) can be combined to give

$$k_{1c}/k_1 = \frac{k_8[CH_3CHO] + k_2[H_2O] + k_6[N_2O]}{2k_2[H_2O]} \times \frac{0.75k_{11}[CH_4]}{k_{11}[CH_4] + k_6[N_2O]} \frac{[CH_3]_{1c}}{[CH_3]_{11a}} \quad (13)$$

The left-hand side of eq 13 is the yield of channel 1c. The ratio of the two CH_3 concentrations in eq 13 can be determined. Provided that $[N_2O]$ and the excimer power are the same for the two measurements,

$$\frac{[CH_3]_{1c}}{[CH_3]_{11a}} = \frac{A_e(CH_3 \text{ with } N_2O, H_2O, CH_3CHO)}{A_e(CH_3 \text{ with } N_2O, CH_4)} \quad (14)$$

Figure 9 shows the CH_3 signal produced in the presence of CH_4 at the N_2O concentration used for measurement and Figure 10 shows the CH_3 signal interpreted in terms of % yield of channel (1c) through eq 14 for three initial acetaldehyde concentrations. The initial rapid rise in yield that takes place in less than 5 μs cannot be from reaction 1 because the 1/e rise time for reaction 1 would be of the order of 100 μs at these $[CH_3CHO]$ concentrations. The smaller slower rising signals, which correspond to about a 2% yield, can be from channel (1c). As indicated by the horizontal lines in Figure 10, reaction 8 accounts for some of the rapid rising signal, but generally less than half of it. A somewhat improbable, but interesting, explanation for the remaining rapidly rising CH_3 signal is that some OH is

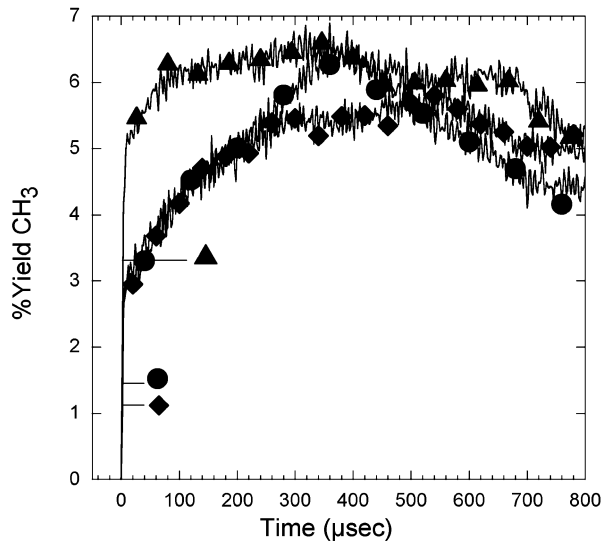

Figure 10. CH_3 signal at 3154.747 cm^{-1} produced in the water, acetaldehyde, nitrous oxide system expressed as % yield of channel (1c). Conditions: He flow 1000 sccm; $P(N_2O) \sim 414$ mTorr; $P(H_2O) \sim 1.2$ Torr; $P(tot) \sim 13.6$ Torr; excimer ~ 135 mJ. Partial pressures of CH_3CHO: (●) 39 mTorr; (▲) 117 mTorr; (◆) 28 mTorr. The horizontal lines with a symbol next to them are the approximate expected CH_3 yields from the $O(^1D) + CH_3CHO$ reaction for the corresponding conditions.

produced vibrationally excited and reacts more rapidly to produce preferentially CH_3.

(3) Atomic Hydrogen. This species could not be observed directly, but evidence for its formation was sought by looking for D_2O. The reaction scheme employed was

$$NO_2 + h\nu(193\text{ nm}) \rightarrow NO + O(^1D) \quad (4)$$

$$O(^1D) + H_2O \rightarrow 2OH \quad (2)$$

$$OH + CD_3CDO \rightarrow D + CD_3COOH \quad (1d')$$

$$D + NO_2 \rightarrow NO + OD \quad (7')$$

$$OD + CD_3CDO \rightarrow D_2O + CD_3CO \quad (1a')$$

so that the D produced by reaction 1d′ is converted quantitatively to a D_2O, which was the species observed. In this scheme, the assumption is made that a D atom rather than an H atom is released in (1d′); this seems reasonable because the OH bond is stronger than the aldehydic CD bond.

To quantify this, it was not necessary to know the D_2O absorption cross-section because the D_2O signal equivalent to the original OH concentration could be obtained by replacing the H_2O by about one Torr of D_2. One $O(^1D)$ is converted into OD by the reaction

$$O(^1D) + D_2 \rightarrow D + OD \quad (15)$$

then the D atom is converted into OD by (7′). Ultimately, essentially all of the OD is converted into D_2O by (1a′) in near 100% yield.

Of course, the same kind of correction for the interception of $O(^1D)$ by acetaldehyde must be made here as was the case for the determination of the CH_3 yield above. On a relative scale, this is not a small correction, because we observed that a large fraction (near 100%) of the reaction of $O(^1D)$ with CD_3CDO produces D_2O in the NO_2/CD_3CDO system whereas the yield of channel (1d′) is small.

$O(^3P)$ is produced in about 45% yield by the photolysis of NO_2. An additional correction must be made for the reaction of $O(^3P)$ with acetaldehyde to produce OD.

$$O(^3P) + CD_3CDO \rightarrow OD + CD_3CO \quad (16)$$

($k_{16} = 4.4 \times 10^{-13}$ cm^3 s^{-1})[15] At CD_3CDO concentrations comparable to the NO_2 concentration, most of the $O(^3P)$ reacts with NO_2

$$O(^3P) + NO_2 \rightarrow O_2 + NO \quad (17)$$

($k_{17} = 9.7 \times 10^{-12}$ cm^3 s^{-1})[19] In addition, NO_2 reacts with CD_3CO[21]

$$CD_3CO + NO_2 \rightarrow CD_3CO_2 + NO \quad (18a)$$

$$\rightarrow CD_3 + CO_2 + NO \quad (18b)$$

with $k_{18} = 2.5 \times 10^{-11}$ cm^3 s^{-1} for the H isotopic species with an unknown branching ratio between channels (18a) and (18b). In the modeling calculations to be described below, reaction 18 was assumed to go entirely via channel (18b). To our knowledge, nothing is known about the reactions of CD_3CO_2. CD_3 reacts with $O(^3P)$

$$CD_3 + O(^3P) \rightarrow CD_2O + D \quad (19)$$

with a rate constant for the H isotope of[14] $k_{19} = 1.2 \times 10^{-10}$ cm^3 s^{-1}. In addition to these reactions, OH (and OD) reacts (slowly) with NO_2 by a three-body reaction to produce HNO_3.

$$OH + NO_2 + He \rightarrow HNO_3 + He \quad (20)$$

with an effective rate constant under our conditions of 8×10^{-13} cm^3 s^{-1}. Finally the isotope exchange reaction

$$D + OH \rightarrow OD + H \quad (21)$$

is fast ($k_{21} = 5.3 \times 10^{-11}$ cm^3 s^{-1}) and is exoergic.

In summary, there are five different sources of D_2O in the system $CD_3CDO/NO_2/H_2O$ photolyzed at 193 nm: [1] reaction 1d′ followed by (15) followed by (1a′) (the D_2O source of interest); [2] reaction 16 followed by (1a′); [3] the reaction of $O(^1D)$ with CD_3CDO to produce D, which ends up as D_2O, [4] reaction 18b followed by reaction 19 followed by (7′) followed by (1a′), and finally [5] D atoms (from whatever source) exchange with OH via reaction 21 with the OD thus produced going on to D_2O. We have modeled the kinetics of this system of reactions as a function of $[CD_3CDO]$, keeping $[NO_2]$ and $[H_2O]$ constant. As expected, source [1], which is of interest, is almost independent of $[CD_3CDO]$ as all the radical species included except for OH (and OD) and CD_3CO quickly reach a steady state at a low concentration level. D_2O source [2] increases with increasing $[CD_3CDO]$, as the competition between NO_2 and CD_3CDO for $O(^3P)$ would shift toward reaction 16. D_2O source [3] rapidly becomes important as $[CD_3CDO]$ increases. Source [4] is the most uncertain because of the unknown branching ratio of reaction 18 but is also expected to increase with increasing $[CD_3CDO]$. This is because higher acetaldehyde concentrations lead to greater $[CD_3CO]$ at early times and thus higher $[CD_3]$ at early times, resulting in more competition of CD_3 with NO_2 for $O(^3P)$. D_2O source [4] also increases with increasing $[CD_3CDO]$, because the reaction of

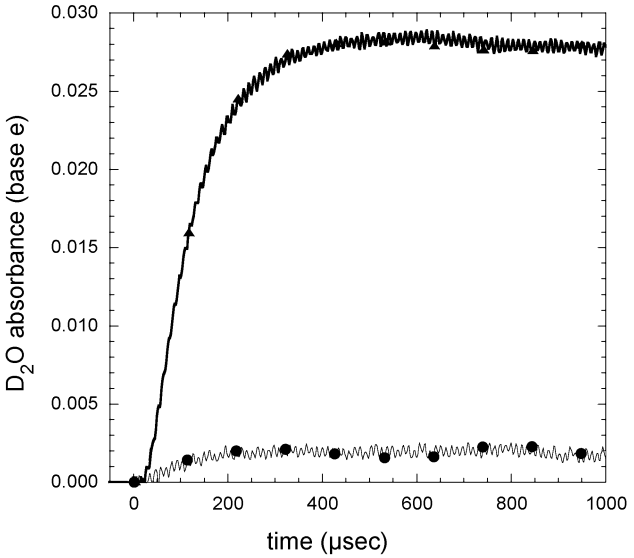

Figure 11. D_2O absorbance at 2711.2171 cm^{-1} with excess water (●) compared with D_2O absorbance with excess D_2 (▲). Conditions: He flow 1000 sccm; $P(NO_2) \sim 33$ mTorr; excimer 110 mJ; (●) $P(CD_3CDO) = 20$ mTorr, $P(H_2O) = 1.3$ Torr, $P(\text{tot}) = 14.1$ Torr; (▲) $P(CD_3CDO) = 25$ mTorr, $P(D_2) = 1.3$ Torr, $P(\text{tot}) = 13.3$ Torr.

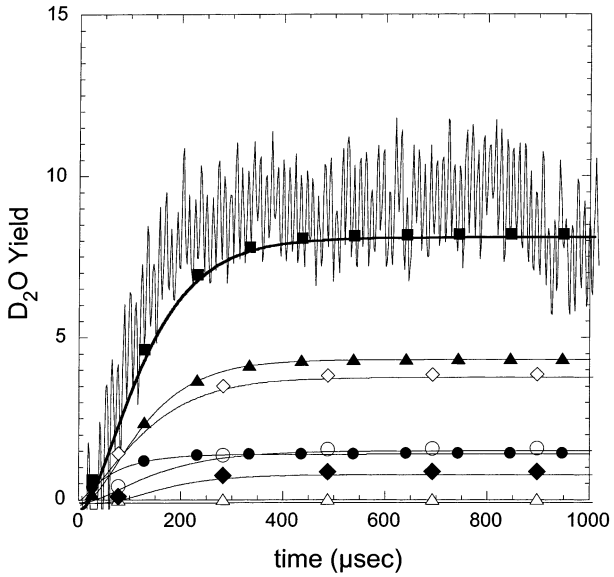

Figure 12. D_2O absorbance of Figure 11 converted to % yield of D_2O interpreted as the D atom yield for the reaction OH + CD_3CDO by dividing the trace with excess water of Figure 11 by the final D_2O absorbance with excess D_2 of Figure 11. Predicted D_2O concentrations for the conditions of Figure 11: (■) sum of assumed 5% yield of D_2O from reaction 1d signal (source [1]) and all artifact sources; (▲) apparent yield in the absence of artifact sources when 5% yield of D from OH + CD_3CDO channel is assumed (1d) is assumed (source [1]); (◇) sum of artifact sources of D_2O; (○) D_2O from O + CD_3CDO (source [2]); (●) D_2O from $O(^1D)$ + CD_3CDO (source [3]); (◆) D_2O from CD_3CO reactions (source [4]); (△) D_2O from D + OH → OD+ H (source [5]).

$O(^1D)$ with CH_3CHO is known to produce about 50% yield of CH_3. Fortunately, [4] is a small D_2O source because most of the CD_3 produced reacts with NO_2 producing CD_3O + NO and CD_3O ultimately reacts with NO_2 to form an adduct. D_2O source [5] has no net effect on the D_2O yield.

Typically, the reaction system contained ~30 mTorr of NO_2, ~1 Torr of H_2O, and various pressures of CD_3CDO in the range 20−40 mTorr. As described above, the major artifact sources [2] and [3] increase in importance as [CD_3CDO] increases. Thus, although observations were made at several CD_3CDO concentrations, we choose to describe the results for the lowest [CD_3CDO]. Figure 11 shows a trace of the experimental absorbance as a function of time at a pressure of CD_3CDO at the low end of the range. (Note: Although the acetaldehyde-d_4 sample was contaminated with D_2O, there was negligible background D_2O absorption, because the large H_2O excess converted all D_2O into HDO.) Figure 11 also illustrates the observed absorbance of D_2O from photolysis of NO_2 in the presence of D_2. Contamination of the acetaldehyde-d_4 sample with D_2O does give rise to a background absorption in this calibration process. However, the transient D_2O signal is much larger here making the effect of D_2O background absorption upon the D_2O transient small.

Figure 12 shows the D_2O signal in terms of % yield of D_2O. In this figure, the D_2O absorbance has been converted to an apparent D_2O yield by dividing the D_2O signal from the $H_2O/NO_2/CD_3CDO$ system by the D_2O signal from $D_2/NO_2/CD_3CDO$ system of Figure 11. This apparent D_2O yield arises from several sources for both systems. These sources were modeled using the rate constants of Table 1 and the initial concentrations of Table 2. In the case of the $D_2/NO_2/CD_3CDO$ system, sources other than (1a′) are only about 5% of the total D_2O signal, but in the case of the $H_2O/NO_2/CD_3CDO$ system, the sources ([2]−[4]), which are unrelated to channel (1d′), are calculated to give rise in total to about half the apparent D_2O yield. The apparent D_2O yield from (1d′) can be well fitted as shown in Figure 12 by assuming a 5% yield of D from the reaction OH + CD_3CDO (1d′), but the uncertainty is large. In summary, we are far from certain that reaction 1 produces any D and can only say that the D atom yield (1d′) is between 0 and 10% with our best estimate about 5%.

TABLE 1: Reaction Scheme Used To Model the D_2O Signals of Figure 12

reaction	k (cm^3 $molecules^{-1}$ s^{-1})
Reactions Common to the $H_2O/NO_2/CD_3CDO$ and $D_2/NO_2/CD_3CDO$ Systems	
$O(^1D) + CD_3CDO \rightarrow D$ + other products	3.2×10^{-10}
$O(^1D) + NO_2 \rightarrow O_2 + NO$	1.1×10^{-10}
$O + NO_2 \rightarrow O_2 + NO$	9.7×10^{-12}
$D + NO_2 \rightarrow OD + NO$	1.4×10^{-10}
$O + CD_3CDO \rightarrow OD + CD_3CO$	4.0×10^{-13}
$OD + CD_3CDO \rightarrow CD_3CO + D_2O$	1.6×10^{-11}
$OD + NO_2 \rightarrow DNO_3$	2.2×10^{-12}
$CD_3CO + NO_2 \rightarrow CD_3$ + other products	2.5×10^{-11}
$CD_3 + O \rightarrow D + D_2CO$	1.2×10^{-10}
$CD_3 + CD_3 \rightarrow C_2D_6$	4.2×10^{-11}
$CD_3 + NO_2 \rightarrow CD_3O + NO$	2.4×10^{-11}
$CD_3O + O \rightarrow CD_3 + O_2$	2×10^{-11}
$CD_3O + NO_2 \rightarrow$ adduct	2×10^{-11}
Reactions Unique to the $H_2O/NO_2/CD_3CDO$ System	
$O(^1D) + H_2O \rightarrow OH + OH$	2.2×10^{-10}
$OH + CD_3CDO \rightarrow D$ + other products	0.8×10^{-12}
$OH + CD_3CDO \rightarrow HDO + CD_3CO$	1.5×10^{-11}
$OH + NO_2 \rightarrow HNO_3$	2.2×10^{-12}
$D + OH \rightarrow OD + H$	5.3×10^{-11}
$H + NO_2 \rightarrow OH + NO$	1.4×10^{-10}
Reaction Unique to the $D_2/NO_2/CD_3CDO$ System	
$O(^1D) + D_2 \rightarrow OD + D$	1.1×10^{-10}

(b) OH + CH_3CHO Rate Constant. The rate constant of reaction 1 is well established. As a check primarily of our ability to measure acetaldehyde flow rates, we have remeasured the rate of (1) using the O_3 system, keeping the O_3 and water concentrations constant and varying the acetaldehyde concentration in the standard pseudo-first-order kinetics method where the exponential decay constant of OH is measured as a function

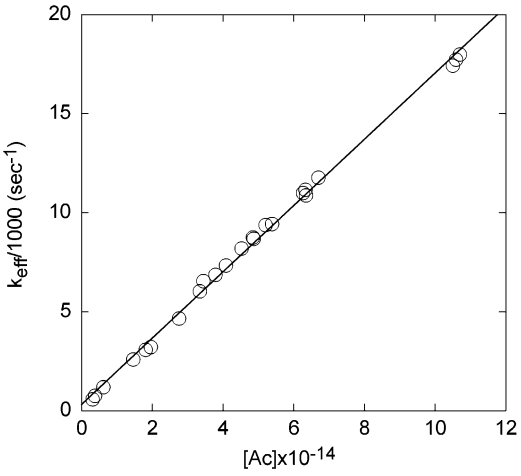

Figure 13. Decay rate of OH plotted as a function of the acetaldehyde concentration. The slope of this line yields a value of 1.67×10^{-11} cm^3 s^{-1} for the rate of the reaction between OH and CH_3CHO.

TABLE 2: Initial Concentrations Used To Model the Data of Figure 12[a]

species	concentration (molecules/cm^3)
Concentrations Common to the $H_2O/NO_2/CD_3CDO$ and $D_2/NO_2/CD_3CDO$ Systems	
CD_3CDO	8.02×10^{14}
NO_2	1.077×10^{15}
$O(^1D)$	0.617×10^{13}
$O(^3P)$	0.617×10^{13}
Concentration Unique to the $H_2O/NO_2/CD_3CDO$ System[b]	
H_2O	4.265×10^{16}
Concentration Unique to the $D_2/NO_2/CD_3CDO$ System[b]	
D_2	4.32×10^{16}

[a] All concentrations not listed were initially zero. [b] Otherwise zero.

of acetaldehyde concentration. Figure 13 shows the plot of the decay rate of OH as a function of the concentration of acetaldehyde. The rate constant obtained from the slope of this line is 1.67×10^{-11} cm^3 s^{-1}, a value somewhat higher than the most recent measurement (1.45×10^{-11} cm^3 s^{-1}) of Tyndall et al.[22] but similar to the recommended evaluated rate constant (1.6×10^{-11} cm^3 s^{-1}) of a recent compilation.[3]

(c) Secondary Reaction. Considerable quantities of CH_3 were observed in the reaction of OH with CH_3CHO when O_3 was used as the $O(^1D)$ source. A time trace of this CH_3 rise is shown in Figure 14. As can be seen in the inset in Figure 14, a small amount of CH_3 is produced rapidly and directly by the reaction of $O(^1D)$ with CH_3CHO, but the much larger, more slowly growing CH_3 signal of Figure 14 can only be accounted for by a new reaction. The rate of growth of CH_3 was unaffected by changes in $[CH_3CHO]$, but increased as $[O_3]$ increased, indicating that CH_3 was being produced by a secondary reaction involving either ozone or a species formed from the photolysis of ozone. The large excess of water ensures that virtually all the $O(^1D)$ produced is converted to OH within 1 μs. At appropriate moderate $[CH_3CHO]$ and $[O_3]$, the decay time of OH can be made considerably shorter, e.g., ~40 μs than the rise time of CH_3, e.g., ~200 μs. In that situation, after the disappearance of OH, the only species present in appreciable concentration are H_2O, O_3, and CH_3CO. Quantitative measurements quickly established that the secondary reaction must involve ozone itself. The CH_3 is almost certainly formed by a reaction of CH_3CO (believed to be the *major* primary product of reaction 1 together with water) with ozone and this secondary

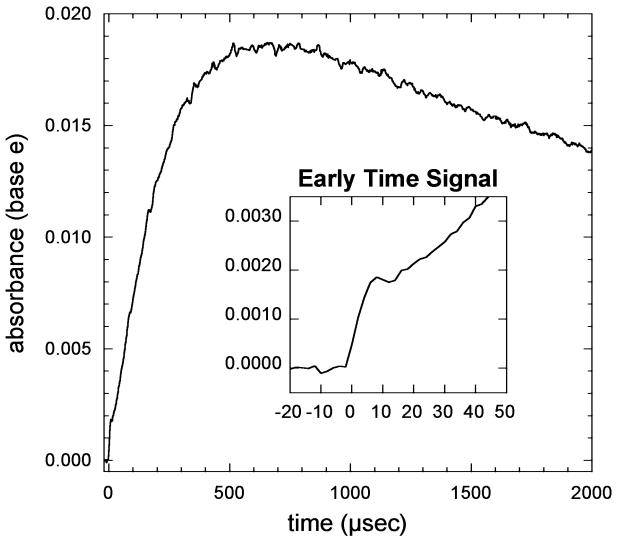

Figure 14. CH_3 signal observed at 3154.747 cm^{-1} in the reaction between OH and CH_3CHO when O_3 was used as the source of $O(^1D)$. The inset shows the small initial rise resulting from the reaction of CH_3CHO with $O(^1D)$. Conditions: He flow 3000 sccm; P(tot) = 22.2 Torr; $P(O_3)$ = 2.78 mTorr; $P(CH_3CHO)$ = 58.5 mTorr; $P(H_2O)$ ~ 1Torr.

reaction producing CH_3 must be (22a)

$$CH_3CO + O_3 \rightarrow CH_3 + CO_2 + O_2 \qquad (22a)$$

$$CH_3CO + O_3 \rightarrow CH_3CO_2 + O_2 \qquad (22b)$$

The concentration of $O(^1D)$ produced under the conditions of Figure 14 can be ascertained by replacing the CH_3CHO and H_2O with a large excess of CH_4 and observing the time behavior of the resulting CH_3 signal. All pertinent rate constants for the CH_4,O_3 system are known as are the initial concentrations of the reagents. Table 3 gives the rate constants used in modeling this system and Table 4 gives the initial concentrations used. The amount of O_3 photolyzed producing $O(^1D)$, i.e., $[O(^1D)]_0$ and $[O_3]_0 = [O_3]_{init} - [O(^1D)]_0$, used in the model was adjusted to match experimental time behavior of the CH_3 signal. Figure 15 shows resulting fit of the time behavior. A factor, C_v (=3.75 $\times 10^{15}$ molecule cm^{-3}), for converting CH_3 absorbance into $[CH_3]$ in our system can then be calculated from the ratio of the ordinate scales of Figure 15.

The $[CH_3]$ for the data of Figure 14 is shown in Figure 16. This was fitted by the reaction model of Tables 3 and 4 by adjusting the rates of reactions 22a and 22b with the result that $k_{22a} = 1.35 \times 10^{-11}$ and $k_{22b} = 3.25 \times 10^{-11}$ cm^3 s^{-1}. It is difficult to estimate the uncertainties in these numbers, because they depend on the uncertainties of all other rate constants built into the model as well as the uncertainties in initial conditions. Even though a change of 0.05×10^{-11} cm^3 s^{-1} creates significant disagreement between model and experiment, the actual uncertainty in the rate is probably $\sim 0.5 \times 10^{-11}$ cm^3 s^{-1}. These rate constants give an overall rate, $k_{22} = 4.60 \times 10^{-11}$ cm^3 s^{-1} and branching ratio into CH_3 or reaction 22a of 29%. Simply dividing the maximum observed $[CH_3]$ in Figure 16 by $2[O(^1D)]_0$ gives an 18% branching ratio. This number is lower than the true branching ratio, because CH_3 has already been reduced by reaction with itself and with OH.

The value of the rate constant for reaction 8 (CH_3CHO + $O(^1D)$) is somewhat uncertain and $[H_2O]_0$ was poorly known for these dataset. The primary effect of k_8 and $[H_2O]_0$ is to change the magnitude of the initial early rise (in opposite

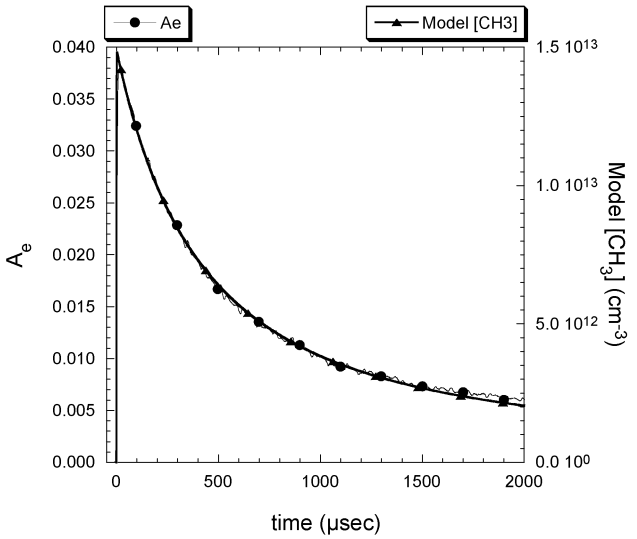

Figure 15. CH_3 signal at 3154.747 cm^{-1} observed (●) in the reaction between $O(^1D)$ and CH_4 compared with the result (▲) of modeling using the reaction scheme of Table 3 and the concentrations of the CH_4 system of Table 4. The concentration of $O(^1D)$ in the model was adjusted for the best match between the observed and calculated time dependence. The two curves can be distinguished only at the longest times.

TABLE 3: Reaction Scheme Used To Model the CH_3 Signals in the O_3 System

reaction	k (cm^3 $molecules^{-1}$ s^{-1})
Reactions Common to CH_4 and CH_3CHO Systems	
$CH_3 + CH_3 \rightarrow C_2H_6$	3.7×10^{-11}
$O(^1D) + O_3 \rightarrow O_2 + O_2$	1.2×10^{-10}
$O(^1D) + O_3 \rightarrow O_2 + O + O$	1.2×10^{-10}
$OH + CH_3 \rightarrow$ products	8.0×10^{-11}
$O + CH_3 \rightarrow$ products	1.2×10^{-10}
$O_3 + CH_3 \rightarrow$ products	2.5×10^{-12}
CH_3CHO System Reactions	
$O(^1D) + H_2O \rightarrow OH + OH$	2.2×10^{-10}
$O(^1D) + CH_3CHO \rightarrow$ non-CH_3 products	1.5×10^{-10}
$O(^1D) + CH_3CHO \rightarrow CH_3 +$ other products	1.5×10^{-10}
$OH + CH_3CHO \rightarrow H_2O + CH_3CO$	1.6×10^{-11}
$CH_3CO + O_3 \rightarrow CH_3 + CO_2 + O_2$	1.4×10^{-11}
$CH_3CO + O_3 \rightarrow CH_3CO_2 + O_2$	3.3×10^{-11}
CH_4 System Reactions	
$O(^1D) + CH_4 \rightarrow CH_3 + OH$	1.1×10^{-10}
$O(^1D) + CH_4 \rightarrow$ other products	0.38×10^{-10}
$OH + CH_4 \rightarrow H_2O + CH_3$	6.4×10^{-15}
$OH + OH \rightarrow H_2O + O$	1.9×10^{-12}

TABLE 4: Initial Concentrations Used To Model the Data of Figures 16 and 17[a]

species	concentration (molecules/cm^3)
O species	
O_3	7×10^{13}
$O(^1D)$	2×10^{13}
CH_4 species[b]	
CH_4	1.75×10^{16}
CH_3CHO species[c]	
CH_3CHO	1.9×10^{15}
H_2O	3×10^{16}

[a] The initial concentrations of all other species referred to in the reaction schemes of Table 1 are zero. [b] Nonzero only in the methane system modeling. [c] Nonzero only in the OH + CH_3CHO system modeling.

directions). Therefore $[H_2O]_0$ has been set in the model to match the rise seen in the inset of Figure 14. The CH_3 produced by reaction 8 may be partially vibrationally excited with the result that this adjustment of $[H_2O]_0$ may be actually unneeded.

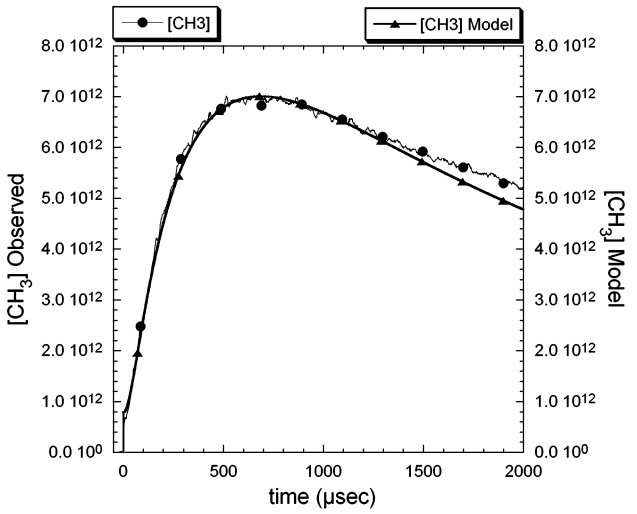

Figure 16. Observed CH_3 signal of Figure 14 converted to $[CH_3]$ (●) by using the ratio of the two ordinate scales of Figure 15 compared with the result (▲) of modeling using the reaction scheme of Table 3 and the concentrations of Table 4. The rate constants of reactions 22a and 22b were adjusted to give the best agreement. The poorly known $[H_2O]$ was adjusted in the model to give good agreement for the very early rise in $[CH_3]$ arising from $O(^1D)$ reacting with CH_3CHO.

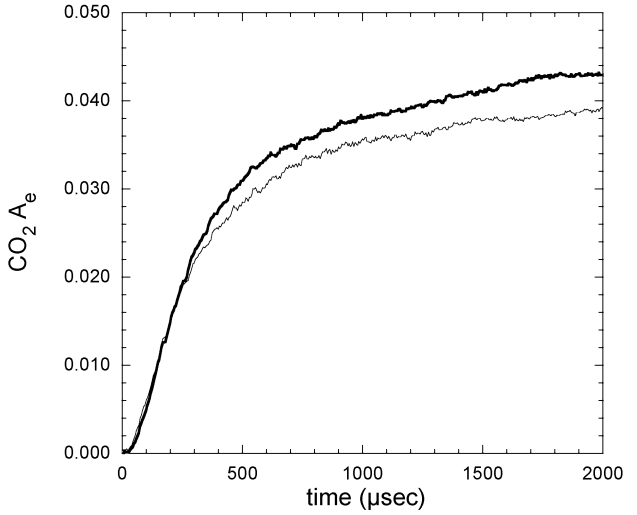

Figure 17. Two signal traces for the CO_2 line at 2385.7742 cm^{-1} under very similar conditions observed from the reaction of O_3 with CH_3CO in the ozone, water, CH_3CHO system.

CO_2 was also observed in the reaction of OH with CH_3CHO using O_3 as the source of $O(^1D)$, as shown in Figure 17. Like methyl, this is a secondary product whose growth rate was measured as being consistently slower than the OH decay rate. In fact, under similar experimental conditions, its concentration/time profile was very similar to that of CH_3. For this reason, it was assumed that CO_2 was formed in reaction 22a.

Discussion

The observations reported here reinforce the conclusions of Michael et al.,[4] Alvarez-Idaboy et al.,[6] and Tyndall et al.[7] that the reaction channel producing water is dominant in the reaction of OH with acetaldehyde. The evidence for the production of small amounts of CH_3 and H atoms through an addition process obtained in the present experiments is tenuous at best. For CH_3 production, most of the CH_3 is produced too rapidly to arise from reaction 1; there is very little (at most 2%) yield of slow CH_3. For H atom production, there appears to be some

production, but considering the uncertainties in modeling the reaction system, the evidence for H atom production in reaction 1 cannot be considered strong.

It would be interesting to carry out these experiments at much lower temperatures. Perhaps the addition products are being formed by stabilization of the prereactive complex proposed by Tyndall et al.[7] in which the hydrogen atom of OH is loosely bonded to the oxygen atom of acetaldehyde. It might be expected that such a complex would be stabilized more effectively at even lower temperatures possibly leading to a greater contribution by addition channels.

Reaction 22 is very similar to the reaction between CH_3CO and NO_2 proposed by Slagle and Gutman.[21]

$$CH_3CO + NO_2 \rightarrow CH_3CO_2 + NO \qquad (18)$$

They state that CH_3 radicals are produced in their system containing CH_3CO, but appear never to write a reaction analogous to reaction 22a. The rate Slagle and Gutman determined for reaction 18 at 295 K is $2.5(\pm 0.6) \times 10^{-11}$, which is similar to the rates given here for reaction 22.

Appendix: Effects of Flash Heating

The base e infrared absorbance is given by

$$A_e(\nu) = -\ln\left(1 - \frac{\Delta I}{I_0}\right) = \sigma(\nu)\,\mathrm{NL} \qquad (A1)$$

and the absorbance integrated over the line is given by

$$\int A_e(\nu)\,d\nu = S\,\mathrm{NL} \qquad (A2)$$

For a Doppler broadened line, the peak absorption cross-section at the line center $\sigma(\nu_0)$ can be related to the integrated absorption S by

$$\sigma(\nu_0) = \frac{S}{\sqrt{\pi}\tilde{\nu}}(c/u) \qquad (A3)$$

with

$$u = \sqrt{\frac{2kT}{m}} \qquad (A4)$$

The integrated absorption S can be related to the vibrational transition moment as

$$S = \frac{4\pi}{3\hbar c}\frac{|\langle v'|\mu|v''\rangle|^2 S_{J'_\tau J''_\tau}}{Q_{\mathrm{int}}} \times [\exp(-E''/(kT)) - \exp(E'/(kT))] \qquad (A5)$$

where Q_{int} is the internal partition function and in our frequency region the term $\exp(-E'/kT)$ can be neglected. The temperature dependence of S is contained in Q_{int} and the Boltzmann factor. For water near room temperature, Q_{int} is proportional to $T^{3/2}$. In the expressions (A1) and (A2), at constant pressure, N is proportional to T^{-1} and L is independent of T. By differentiating the expression for (A2) resulting from substituting (A5) with respect to T, one obtains

$$\frac{d[\ln(\int A_e(\nu)\,d\nu)]}{dT} = -2.5T^{-1} + \frac{E''}{kT^2} \qquad (A6)$$

This function and the corresponding one for $\sigma(\nu_0)$, which differs only in having 2.5 replaced by 3, are plotted in Figure 6. This figure shows that at room-temperature transitions with a lower state energy of less than 514 cm^{-1} decrease in integrated absorbance when the temperature increases whereas those with higher lower state energies increase. The corresponding crossing point for peak absorbance is 617 cm^{-1}.

The HDO line chosen to measure the H_2O yield has a lower state energy of 402.33 cm^{-1}. The expected change in the $\log_e$ of the integrated absorbance at this energy is -0.0018 K^{-1} at room temperature.

Acknowledgment. The work was supported by grants from the Department of Energy and the Robert A. Welch Foundation.

References and Notes

(1) Kleindiest, T. E.; Shepson, P. B.; Smith, D. F.; Hudgens, E. E.; Nero, C. M. C., L. T.; Bufini, J. J.; Claxton, L. D. *Environ. Mol. Mutagen* **1990**, *16*, 70.

(2) Atkinson, R. J.; Lloyd, A. C. *J. Phys. Chem. Ref. Data* **1984**, *13*, 315.

(3) Atkinson, R. J.; Baulch, D. L.; Cox, R. A.; Hampson, R. F.; Kerr, J. A.; Rossi, M. J. *J. Phys. Chem Ref. Data* **1997**, *26*, 521.

(4) Michael, J. V.; Keil, D. G.; Klemm, R. B. *J. Chem. Phys.* **1985**, *83*, 1630.

(5) Taylor, P. H.; Rahman, M. S.; Arif, M.; Dellinger, B.; Marshall, P. *Symp. (Int.) Combust. [Proc.]* **1996**, *26th*, 497.

(6) Alvarez-Idaboy, J. R.; Mora-Diez, N.; Boyd, R. J.; Vivier-Bunge, A. *J. Am. Chem. Soc.* **2001**, *123*, 2018.

(7) Tyndall, G. S.; Orlando, J. J.; Wallington, T. J.; Hurley, M. D.; Goto, M.; Kawasaki, M. *Phys. Chem. Chem. Phys.* **2002**, *4*, 2189.

(8) Sun, F.; DeSain, J. D.; Scott, G.; Hung, P. Y.; Thompson, R. I.; Glass, G. P.; Curl, R. F. *J. Phys. Chem. A* **2001**, *105*, 6121.

(9) Pilgrim, J. S.; Jennings, R. T.; Taatjes, C. A. *Rev. Sci. Instrum.* **1997**, *68*, 1875.

(10) Selwyn, G.; Podolske, J.; Johnson, H. J. *Geophys. Res. Lett.* **1977**, *4*, 427.

(11) Zelikoff, M.; Aschenbrand, I. M. *J. Chem. Phys* **1954**, *22*, 1685.

(12) Sun, F.; Glass, G. P.; Curl, R. F. *Chem. Phys. Lett.* **2001**, *337*, 72.

(13) DeMore, W. B.; Sanders, S. P.; Golden, D. M.; Hampson, R. F.; Kurylo, M. J.; Howard, C. J.; Ravishankara, A. R.; Kolb, C. E.; Molina, M. J. Chemical Kinetics and Photochemical Data for Use in Stratospheric Modeling. JPL Publication, California Institute of Technology, 1994.

(14) Atkinson, R. J.; Baulch, D. L.; Cox, R. A.; Hampson, R. F.; Kerr, J. A.; Rossi, M. J. *J. Phys. Chem. Ref. Data* **1999**, *28*, 191.

(15) DeMore, W. B.; Sander, S. P.; Golden, D. M.; Hampson, R. F.; Kurylo, M. J.; Howard, C. J.; Ravishankara, A. R.; Kolb, C. E.; Molina, M. J. Chemical kinetics and photochemical data for use in stratospheric modeling. Evaluation number 12. JPL Publication, California Institute of Technology, 1997.

(16) Rauche, G. A. *J. Chem. Phys.* **1990**, *92*, 7258.

(17) Heller, D. F.; Moore, C. B. *J. Chem. Phys.* **1970**, *52*, 1005.

(18) Donaldson, D. J.; Leone, S. R. *J. Phys. Chem.* **1987**, *91*, 3128.

(19) Atkinson, R. J.; Baulch, D. L.; Cox, R. A.; Hampson, R. F.; Kerr, J. A.; Rossi, M. J. *J. Phys. Chem. Ref. Data* **1997**, *26*, 1329.

(20) Rothman, L. S.; Barbe, A.; Benner, D. C.; Brown, L. R.; Camy-Peyret, C.; Carleer, M. R.; Chance, K.; Clerbaux, C.; Dana, V.; Devi, V. M.; Fayt, A.; Flaud, J.-M.; Gamache, R. R.; Goldman, A.; Jacquemart, D.; Jucks, K. W.; Lafferty, W. J.; Mandin, J.-Y.; Massiem, S. T.; Nemtchinov, V.; Newnham, D. A.; Perrini, A.; Rinsland, C. P.; Schroeder, J.; Smith, K. M.; Smith, M. A. H.; Tang, K.; Toth, R. A.; Auwera, J. V.; Varanasi, P.; Yoshinoa, K. *J. Quant. Spectrosc. Radiat. Transfer*, in press.

(21) Slagle, I. R.; Gutman, D. *J. Am. Chem. Soc.* **1982**, *104*, 4741.

(22) Tyndall., G. S.; Staffelbach, T. A.; Orlando, J. J.; Calvert, J. G. *IntJ. Chem. Kinet.* **1995**, *27*, 1009.